

# Initial transient structure and chemistry of intergranular glassy films in ferric-oxide doped strontium titanate ceramics

JuanJuan Xing · Hui Gu · Yoon-Uk Heo ·  
Masaki Takeguchi

Received: 30 August 2010 / Accepted: 11 January 2011 / Published online: 26 January 2011  
© Springer Science+Business Media, LLC 2011

**Abstract** Intergranular glassy films (IGFs) often play a key role in the formation of microstructure and the resultant properties in titanate-based materials. In this article, a systematic study of IGF structure and chemistry is reported in  $\text{Fe}_2\text{O}_3$ -doped  $\text{SrTiO}_3$  ceramics sintered under different temperatures and dwelling times. IGFs exhibit a large variation in their thicknesses, although majority of them are still formed by the lower energy {100}, {110}, and {111} planes from one side, which is also true for those grain boundaries (GBs) without IGF and reveals no particular effect of crystallography on IGF width. Furthermore, two trends of IGF chemical composition were found coexisting in each sample, one rich in Ti and the other in Sr, and both containing Fe segregants. The change of sintering temperature did not show significant effect on the distributions for both trends. However, increase of the dwelling time is effective to turn some Sr-rich IGFs to Ti-rich IGF, indicating that the former is in a transient state and the equilibrium IGF has most likely a  $\text{TiO}_2$ -based composition.

## Introduction

In polycrystalline titanate-based ceramics (e.g.,  $\text{SrTiO}_3$  and  $\text{BaTiO}_3$ ), grain boundaries (GBs) often play a key role not only in the development of microstructure but also in the materials' properties [1–3]. As well known, internal interfaces (including GB) can reduce the ionic conductivity especially in doped material systems. This is often attributed to the formation of space-charge layer that compensates the extra charges from dopants or impurities segregating to GB, which may lead to the formation of double Schottky barriers [4–7].

In fact, the formation of GB structure is sensitive to several factors, such as the crystallography or energy of GB plane as well as the interfacial chemical, especially during the microstructure development process. Ernst et al. [8] have analyzed the orientation relationships between neighboring grains in  $\text{SrTiO}_3$ ,  $\text{BaTiO}_3$ , and  $\text{Pb}(\text{Zr}_x\text{Ti}_{1-x})\text{O}_3$  ceramics, and revealed a significant preference for  $\Sigma 3$  relation. Saylor et al. [9] have reported that more boundaries were terminated by low-energy {100} planes than other planes in polycrystalline  $\text{SrTiO}_3$  materials. In  $\text{Bi}_2\text{O}_3$ -doped ( $\text{Sr},\text{Ba})\text{TiO}_3$  ceramics, two types of GB structures,  $\text{TiO}_2$ -rich intergranular glassy films (IGFs) and nano-Bi precipitates were observed in the same materials due to the local amount of Ti at GB during the cooling [10].

Although considerable researchers devoted their efforts to the study of GB in Fe-doped  $\text{SrTiO}_3$  as a model system for the accepter-doped perovskite, most of them focused on GBs in bicrystals which might not represent GBs in polycrystalline materials [11–13]. Indeed, IGFs were often observed in various ceramics samples which exhibited also quite different dopant segregation behaviors as compared to these coherently structured GBs [14–16], and there is no exception for  $\text{SrTiO}_3$  [17, 18]. In this regard, we present

J. Xing (✉) · H. Gu  
State Key Lab of High Performance Ceramics and Super-Fine Microstructures, Shanghai Institute of Ceramics, Chinese Academy of Sciences, Shanghai 200050, China  
e-mail: XING.Juanjuan@nims.go.jp

J. Xing · M. Takeguchi  
Advanced Electron Microscopy Group, Advanced Nano-Characterization Center, National Institute for Materials Science, 3-13 Sakura, Tsukuba 305-0003, Japan

Y.-U. Heo  
Research Facility Center, Graduate Institute for Ferrous Technology, Pohang University of Science and Technology, San 31, Hyoja dang, Pohang 790-784, Korea

here a systematic study of IGF structures and chemistries in a series of  $\text{Fe}_2\text{O}_3$ -doped  $\text{SrTiO}_3$  ceramics by utilizing principally the analytical electron microscopy. Strong variations of IGF structure and chemistry were found and their orientation relationships were examined.

## Experimental

The ceramic materials studied here were fabricated from high-purity  $\text{SrTiO}_3$  and  $\text{Fe}_2\text{O}_3$  (AR: analytical reagent; Sinopharm Chemical Reagent Co. Ltd, China) powders by conventional synthesis method. The powders of  $\text{SrTiO}_3$  with 0.8 mol% of  $\text{Fe}_2\text{O}_3$  additives were milled in ethanol for 24 h in a planetary ball-mill machine and were dried afterward. 5 wt% of PVB (polyvinyl butyral) was added as the binder before the powders were pressed into disks with

a diameter of 15 mm and thickness of  $\sim 3$  mm. These disks were sintered in air for 4 h at 1350, 1410, and 1450 °C, respectively. Accordingly, the sintered ceramic samples were named after SF-1, SF-2, and SF-3. For the sake of comparing the effect of sintering time, a sample was sintered at 1410 °C but held for 10 h, which was given the name of SF-2\*.

Transmission electron microscopy (TEM) specimens were prepared by conventional specimen preparation techniques, including mechanical cutting, grinding, polishing, dimple-grinding, and ion-beam milling. TEM imaging was carried out with JEM-2010 and JEM-3000F electron microscopes (JEOL Co., Japan). The cation concentrations were measured quantitatively by energy dispersive X-ray spectroscopy (EDXS) system (Link/ISIS, Oxford Instruments, UK), which was attached to JEM2010. The actual probe for EDXS analysis was

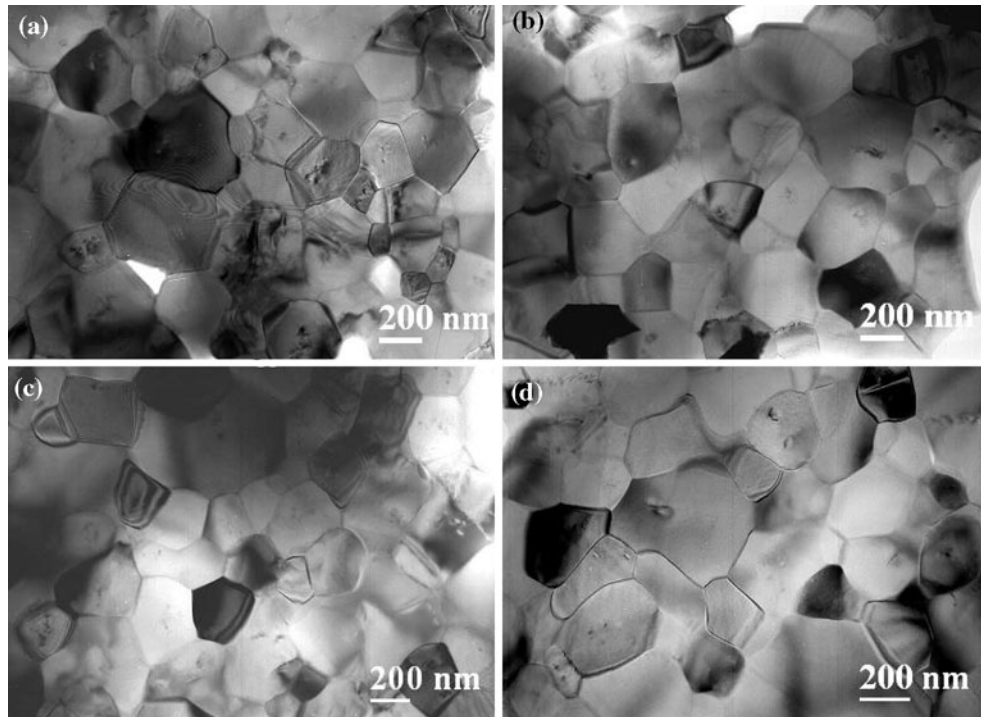


**Fig. 1** TEM images of microstructures in  $\text{Fe}_2\text{O}_3$ -doped  $\text{SrTiO}_3$  ceramics: **a** SF-1, **b** SF-2, **c** SF-2\*, **d** SF-3

**Table 1** Summary of sintering conditions, microstructural, and micro-chemical parameters in  $\text{Fe}_2\text{O}_3$ -doped  $\text{SrTiO}_3$  ceramics

Sample	Temp. (°C)	Time (h)	Grain size (nm)	Fe:Sr ratio	Ti:Sr ratio	$\Gamma_{\text{Fe}}$	$\Gamma_{\text{Ti}}$
SF-1	1350	4	$260 \pm 130$	$0.003 \pm 0.002$	$0.979 \pm 0.054$	$8.11 \pm 3.34$	$-8.61 \pm 16.11$
SF-2	1410	4	$285 \pm 110$	$0.003 \pm 0.003$	$0.984 \pm 0.063$	$7.17 \pm 3.54$	$-9.45 \pm 14.57$
SF-2*	1410	10	$275 \pm 110$	$0.003 \pm 0.002$	$1.006 \pm 0.078$	$7.72 \pm 3.11$	$1.08 \pm 15.99$
SF-3	1450	4	$280 \pm 110$	$0.006 \pm 0.005$	$1.004 \pm 0.089$	$9.04 \pm 3.77$	$-6.41 \pm 15.59$

measured to be 35 nm, which gave sufficient current to acquire spectra. The elemental quantification was based on the Cliff–Lorimer equation with the standard-less routine and using ZAF corrections. Measurement of

dopant segregation to GB was performed by spot mode with positioning the probe on and off GBs [15, 19]. Excesses of segregants were quantified according to [10, 15].

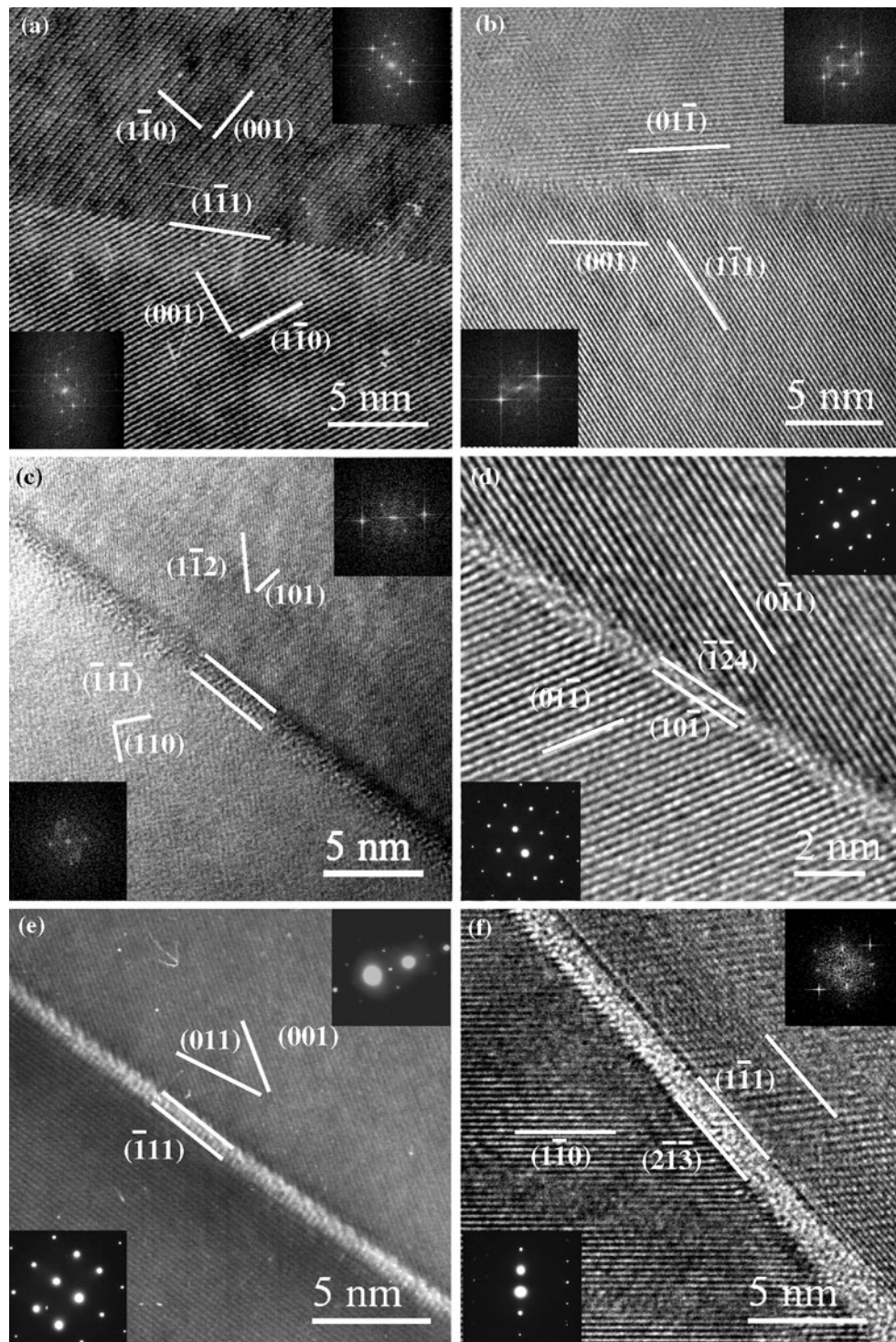


**Fig. 2** HRTEM images of **a–b** GB without IGF, and **c–f** GB with IGF, all sampled in the sample SF-3. Insets are the corresponding fast Fourier transform (FFT) or selected area diffraction (SAD) patterns of

neighboring grains, which were utilized to identify the interface planes of each IGF in addition to HRTEM

## Results and discussion

### Common microstructure and different GB structures

Typical TEM images from the  $\text{Fe}_2\text{O}_3$ -doped  $\text{SrTiO}_3$  samples are shown in Fig. 1. All the samples exhibit the uniform microstructures by equiaxed grains with similar average grain sizes all close to 300 nm, as given in Table 1. The common microstructure characters indicate that neither sintering temperature nor sintering time has significant effect on the grain growth, which provide a simple system to study the behaviors of GB structures during sintering, without involving any effect from grain growth.

GB structures were characterized by high-resolution transmission electron microscopy (HRTEM), and strong variation in GB structures was found in each sample. Taking the sample SF-3, for example, some GBs have no IGF to form either coherent or incoherent interfaces (Fig. 2a, b); most GBs are covered with IGFs, but in different thicknesses (Fig. 2c–f). Such a variety of GB structures and variation in IGF width are common for all these samples. The grain surface planes of IGF could also be determined either from HRTEM directly (with the help of fast Fourier transformed diffractogram) or from electron diffraction [15]. {100}, {110}, and {111} planes are rather common as the interfacial planes for IGFs. Therefore, we attempted a systematic correlation of IGF thickness with the grain surface structures in SF-3 sample. By removing the lattice fringes from the HRTEM image via Fourier filtering to highlight the amorphous structure [14], the thickness of each IGF was measured. The interfacial planes of these GBs are summarized in Table 2 and arranged in the order of IGF thickness that varying from 0.5 to 2.6 nm. It is worthy of mentioning that the measured width of IGF using a non-corrected microscope could be slightly larger due to the delocalization effect at interfaces. This may make the uncertainty in IGF thickness exceeding the widely believed 0.1 nm, but on the other hand, this should still be less than 0.2–0.3 nm [20, 21], which validates the analysis in this study. Among 15 GBs with IGF investigated in SF-3, there are five cases that one interfacial plane to be {100} plane, six cases to be {110} plane, three cases to be {111} plane. It seems that, comparing with the other planes with higher indexes, the {100}, {110}, and {111} planes were preferred as the habit interfacial planes between the amorphous and the crystalline structures, at least from one side of the IGF. Moreover, these low-index interfacial planes generally appear as atomically flat, as shown in Fig. 2e, f, while the high-index interfacial planes do not, as shown in Fig. 2c, which is consistent with the observations from Chung et al. [22]. These results may also be due to the fact that these low-index planes are much

easier to be targeted using HRTEM technique that prefers flat interfaces.

The formation of IGFs with varying thicknesses could be rationalized as a behavior due to the change of GB energy with different interfacial crystallographies. Saylor et al. proposed that the GB energy was correlated to the surface energies of the planes on either side of the boundary and that the binding energy between the two surfaces was approximately constant. Consequently, the GB population in  $\text{SrTiO}_3$  was correlated to the sum of the energies of the surfaces comprising the boundary, and the most frequently observed boundaries should have the lowest energies [9]. Holm et al. [23] have shown that the population of GBs with relatively a low energy increased, while the population of high energy GBs decreased during the grain growth. Therefore, our results show that {100}, {110}, and {111} planes are common to be the interfacial planes between IGFs and the adjacent grains is consistent with this trend. Luo [24] has demonstrated the anisotropic wetting of  $\text{Bi}_2\text{O}_3$ -enriched surface amorphous films on  $\text{ZnO}$ . He ascribed the anisotropic effect to the induced order between the  $\text{ZnO}$  surface structures and the bismuth oxide units constituting the amorphous film. In Table 2, the two GBs with wide IGF over 2 nm both take {111} planes as one of the two interfacial planes. While for IGFs with thickness less than 1 nm, {110} planes prevail as one of the interfacial plane, except GB12 and GB13. In  $\text{SrTiO}_3$  lattice, the (100) plane is alternatively made of  $\text{SrO}$  or  $\text{TiO}_2$

**Table 2** Characteristics of GBs with IGF in SF-3

Analyzed boundaries	Interfacial plane <sup>a</sup>		IGF width (nm)
	Grain 1	Grain 2	
GB1	(111)	–	2.6
GB2	(111)	(010)	2.5
GB3	–	–	2.0
GB4	(110)	(011)	1.4
GB5	(111)	(213)	1.2
GB6	(001)	(112)	1.1
GB7	(001)	–	1.0
GB8	(021)	(213)	1.0
GB9	–	(110)	0.9
GB10	–	(011)	0.8
GB11	(110)	(110)	0.8
GB12	(001)	–	0.8
GB13	–	–	0.7
GB14	(101)	(124)	0.7
GB15	(100)	(101)	0.5

<sup>a</sup> Interfacial planes were determined by the corresponding fast Fourier transform (FFT) or selected area diffraction (SAD) patterns (see text for more details)

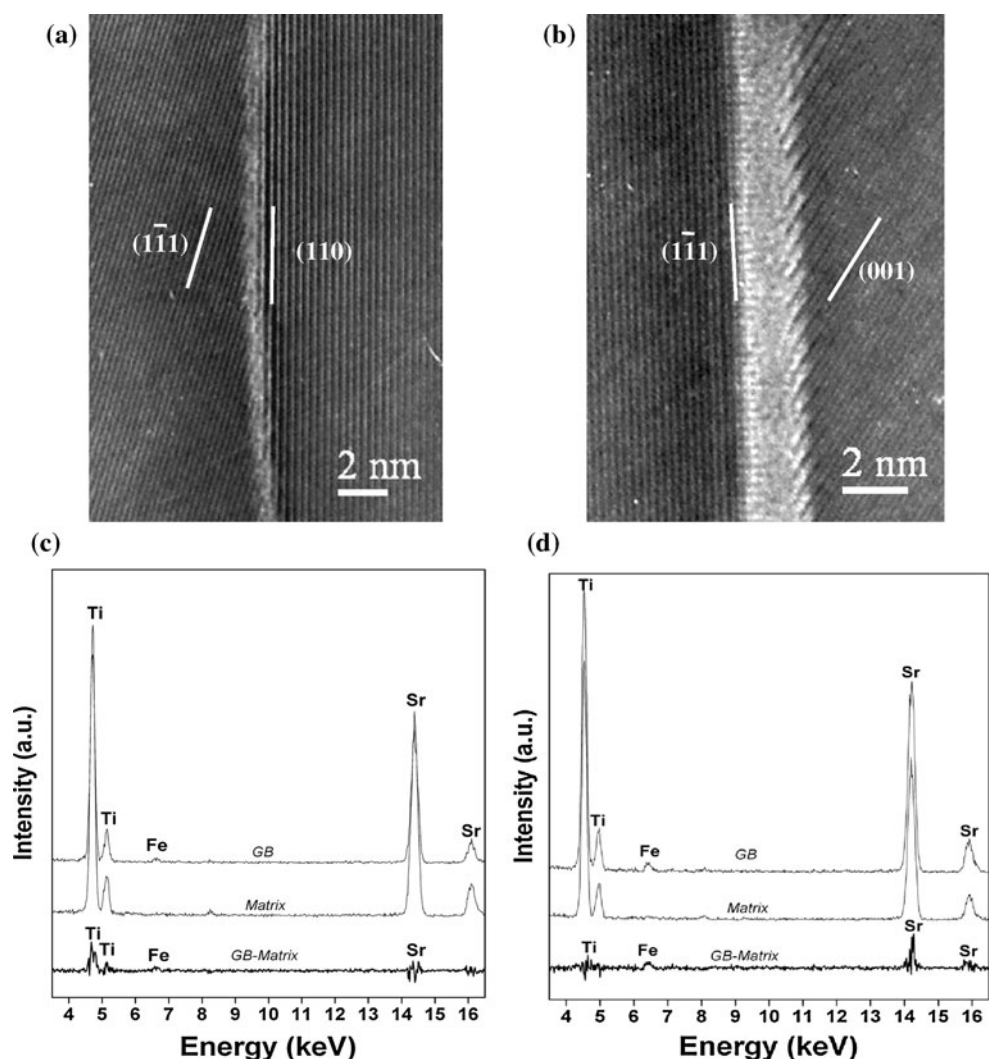
compositions, which is charge-balanced, hence non-polar. The (110) plane is alternatively  $O_2^{4-}$  or  $(SrTiO)^{4+}$  plane, and the (111) plane is  $Ti^{4+}$  or  $(SrO_3)^{4-}$  plane, hence both planes are polar, which may initiate permanent dipole moments at the grain surface [25]. In the actual observation of surface structure (111) terminations were found to be Ti or reduced  $SrO_{3-x}$  [26]. The stoichiometry of SrTiO is likely to be observed for (110) termination [27]. According to the results of Pojani et al. [27], the averaged surface energies  $\bar{E}_s$  is almost independent of the actual surface composition for (111) termination. For (110), the values of  $\bar{E}_s$  are more contrasted and depend upon the surface geometry and stoichiometry.  $\bar{E}_s$  of the stoichiometric SrTiO–O<sub>2</sub> slab is lower than that of (111) termination, which indicates that (110) is relatively more stable than (111). Thus, supposing a common interfacial plane from one side, the GB with (110) as the other interfacial plane should reach the equilibrium state easier than the GB with (111) plane as the second interface. GB2 and GB15 shown in Table 2 are just like the case, which accommodates with

IGF of 2.6 and 0.5 nm, respectively. Nevertheless, it is difficult to draw a conclusion that the thickness of IGF is clearly depend upon the interfacial plane since the statistic is far from sufficient, and it is very difficult to get the complete crystallographic information from both sides of IGF to proceed such assessment.

## Two typical chemistries for IGFs

Segregations of Fe and Ti to GBs were measured by EDXS analysis described in “Experimental.” About 20 GBs were detected in each sample. Since these GBs were selected more or less randomly, GB with or without IGF should all be included and the selection should correspond to a good representation of actual population of GB structures. Solution and segregation data in average are given in the Table 1. It can be seen that Fe solutions in all the samples are very low. Most of  $Fe^{3+}$  dopants are segregated to GBs, which were also found by earlier studies [17, 28]. The excess of  $Fe^{3+}$  at GB exhibits almost no change with

**Fig. 3** Two IGFs with different compositions in SF-3: **a–b** their HRTEM images; **c–d** their EDXS spectra and the processed spatial difference, corresponding to **(a)** and **(b)**, respectively



sintering temperature or sintering time, although it might vary if we increase the level of  $\text{Fe}_2\text{O}_3$  doping, similar to the case of  $\text{Nb}_2\text{O}_5$  doping in  $\text{SrTiO}_3$  ceramics [29]. Yan et al. [30] have discussed the main driving forces for solutes segregation at interfaces as the elastic energy, the electrostatic potential and the dipole interactions. Under the same six-coordinated configurations, the size of  $\text{Fe}^{3+}$  ions (0.065 nm) is quite close to that of  $\text{Ti}^{4+}$  ions (0.061 nm) [31], the elastic energy due to the size mismatch could be neglected. Therefore, the main driving forces for  $\text{Fe}^{3+}$  segregation to GB should be either electrostatic potential and/or dipole coupling.

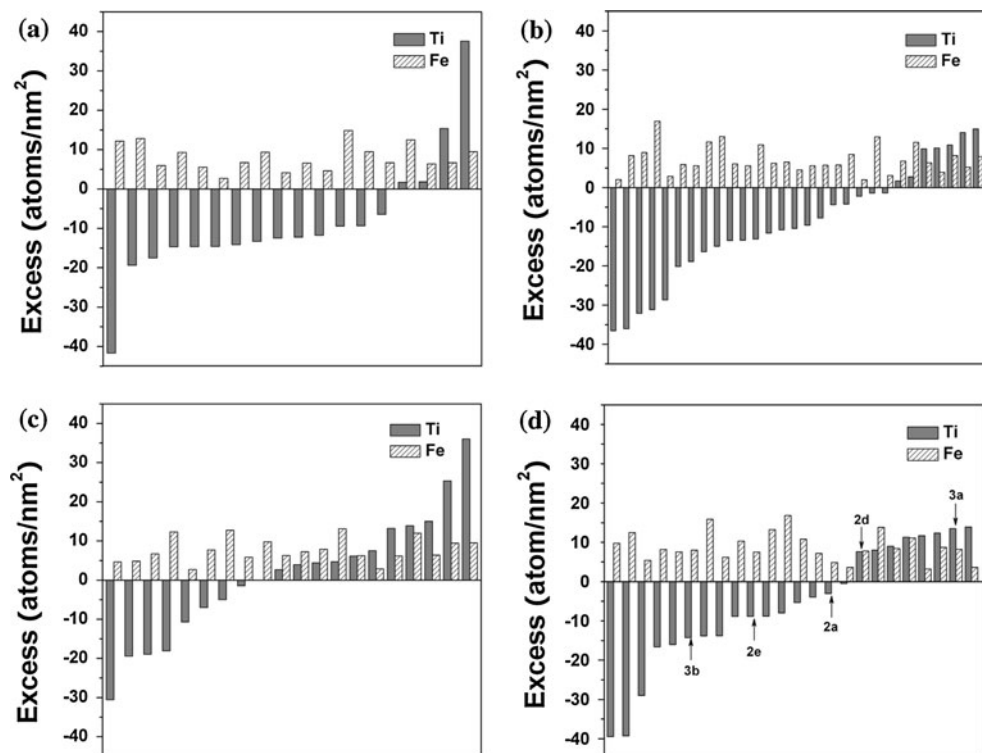
The level of Ti at GB exhibits a quite different behavior from Fe segregation. The excess of Ti varies over a wide range that extends well into negative domains in each sample. The negative excess of Ti corresponds to the lower level of Ti content in GB than in the neighboring grains, indicating a depletion of Ti from GB zone and consequently the enrichment of Sr in GB [10]. Indeed, two kinds of IGF chemistries were detected by utilizing the EDXS spatial difference method [10, 32]. Figure 3a shows the HRTEM image of a thin IGF, from which the spatial difference spectrum (Fig. 3c) reveals that it is abundant in Fe and Ti, which is consistent with the excesses of  $\Gamma_{\text{Fe}} = 8.2$  atoms/nm<sup>2</sup> and  $\Gamma_{\text{Ti}} = 13.5$  atoms/nm<sup>2</sup>. In contrast, the IGF shown in Fig. 3b is composed of excessive Fe and Sr as revealed in Fig. 3d by the same spectral processing, which corresponds to the excesses of  $\Gamma_{\text{Fe}} = 8.0$  atoms/nm<sup>2</sup> and

$\Gamma_{\text{Ti}} = -14.2$  atoms/nm<sup>2</sup>. Recently, Shih et al. [33] have also reported the Sr-rich GB in  $\text{SrTiO}_3$ , which was associated with the abnormally grown grains but in the absence of IGF. Fe segregation in our case might contribute to a solute-drag effect to hinder the grain growth [34]. Nevertheless, the observation of Sr-rich IGF is still a puzzle that is reported for the first time in  $\text{SrTiO}_3$  materials to our best knowledge.

#### Evolution of IGF chemistry

To further understand the distribution of GB chemistries, we plot Ti excess in correlation with Fe excess from the GBs, as shown separately in each sample in Fig. 4; GBs already shown in Figs. 2 and 3 from SF-3 are marked by arrows in Fig. 4d. Insensitive to the sintering temperature, it is common to exhibit a wide range of distribution for GB chemistry from Sr- to Ti-rich: the Sr-rich GBs are majority in numbers, while the number of Ti-rich GBs increases slightly with temperature from ~22% in SF-1 to ~33% in SF-3. In contrast, the effect of dwelling time to change the GB chemistry is more remarkable with the population of Ti-rich GBs increasing more than doubled to overtake the Sr-rich GBs, from ~24% in SF-2 to ~55% in SF-2\*. These distributions not only demonstrate a tendency for Sr-rich GB to turn into Ti-rich, they also indicate that, comparing with the sintering temperature, the increase of dwelling time is more effective to facilitate such a trend. Although no IGF

**Fig. 4** Correlated distributions of Ti and Fe excesses from GBs in samples: **a** SF-1, **b** SF-2, **c** SF-2\*, **d** SF-3. Data are arranged in the order of Ti excess; the corresponding GBs and IGFs from SF-3 are marked in **(d)**



was observed, recently Bäurer et al. [35] have also reported a similar trend of Sr-rich GB to change into Ti-rich GB with extended annealing time in  $\text{SrTiO}_3$  materials with  $\text{TiO}_2$ -excess, which is consistent with our case.

The eutectic temperature of  $\text{SrTiO}_3\text{--TiO}_2$  is at 1440 °C [36] and only the sample SF-3 was sintered above this temperature. However, the liquid phase could be formed at about 1200 °C in  $\text{SrO}\text{--Fe}_2\text{O}_3$  system [37], suggesting that all the samples may involve the liquid phase during sintering, at least at the early stage of sintering. Nevertheless, the existence of two typical IGF chemistries and the wide distribution of IGF thickness (0.5–2.6 nm) indicate that the GBs are far from equilibrium, both chemically and structurally, and covered by intergranular liquid to retain even after sintering in all samples. Dillon et al. [38] and Harmer [39] proposed the concept of GB complexion based on their study of alumina, and assumed that abnormal grain growth (AGG) occurs when two or more different GB complexions coexist in the same microstructure. However, no AGG phenomenon occurred although GB with and without IGF coexist in this study. Therefore, an extensive evolution of IGF chemistry occurred before the start of any micro-structural evolution in our case. Indeed, a similar situation was reported in low- $\text{TiO}_2$ -doped alumina ceramics with minor- $\text{SiO}_2$  impurities, where the IGF chemistry had also evolved to certain extent to initiate the anisotropic grain growth [40].

## Conclusions

In this study, we have presented a systematic investigation of the structures and chemistries of GBs in a series of  $\text{Fe}_2\text{O}_3$ -doped  $\text{SrTiO}_3$  ceramics sintered with different temperatures or dwelling times. Irrespective of sintering conditions, all the samples exhibit the equiaxial uniform microstructures. It might be related to the strong Fe segregation to GBs. GBs with or without IGF were observed in each sample. IGFs exhibit a large variation in their thicknesses. Majority of them are formed by the lower energy {100}, {110}, and {111} planes from at least one side, which is also true for those GBs without IGF and reveals no particular effect of crystallography on IGF width. Two trends of IGF chemical composition were found coexisting in each sample, one rich in Ti and the other in Sr, and both containing also Fe segregants. Dwelling time is much more effective to turn Sr-rich IGFs to Ti-rich IGF comparing with the sintering time, indicating that the former is in a transient state.

**Acknowledgements** This study was financially supported by the National Natural Science Foundation of China via Grants No. 50525205. The authors appreciate beneficial discussions with Dr. M. Čeh of Jožef Stefan Institute of Slovenia.

## References

- Denk I, Claus J, Maier J (1997) *J Electrochem Soc* 144:3526
- Waser R (1995) *Solid State Ion* 75:89
- Lee SB, Lee JH, Cho PS, Kim DY, Sigle W, Philipp F (2007) *Adv Mater* 19:391
- Hagenbeck R, Waser R (1999) *J Eur Ceram Soc* 19:683
- Chiang YM, Takagi T (1990) *J Am Ceram Soc* 73:3278
- Desu SB, Payne DA (1990) *J Am Ceram Soc* 73:3391
- Yamamoto T, Sato Y, Tanaka T, Hayashi K, Ikuhara Y, Sakuma T (2005) *J Mater Sci* 40:881. doi:[10.1007/s10853-005-6505-4](https://doi.org/10.1007/s10853-005-6505-4)
- Ernst F, Mulvihill ML, Kienzle O, Rühle M (2001) *J Am Ceram Soc* 84:1885
- Saylor DM, Dasher BE, Sano T, Rohrer GS (2004) *J Am Ceram Soc* 87:670
- Xing JJ, Gu H, Gloter A, Shen H, Pan XM, Wang PC (2007) *Acta Mater* 55:5323
- De Souza RA, Fleig J, Maier J, Zhang ZL, Sigle W, Rühle M (2005) *J Appl Phys* 97:5
- Bentham K, Tan GL, DeNoyer LK, French RH, Rühle M (2004) *Phys Rev Lett* 93:227201
- Guo X, Fleig J, Maier J (2002) *Solid State Ion* 154–155:563
- Subramaniam A, Koch CT, Cannon RM, Rühle M (2006) *Mater Sci Eng A* 422:3
- Chi MF, Gu H (2004) *Interface Sci* 12:335
- Chi MF, Gu H, Qian PX, Wang X, Wang PL (2005) *Z Metallkd* 96:486
- Pan X, Gu H, Stemmer S, Rühle M (1996) *Mater Sci Forum* 207–209:421
- Gu H (1997) *Mat Res Soc Symp Proc* 458:115
- Gu H, Cannon RM, Rühle M (1998) *J Mater Res* 13:376
- MacLaren I, Cannon RM, Gülgün MA, Rayisa V, Popescu-Pogripon N, Scheu C, Tffner U, Rühle M (2003) *J Am Ceram Soc* 86:650
- MacLaren I (2004) *Ultramicroscopy* 2004:103
- Chung SY, Kang SL (2003) *Acta Mater* 51:2345
- Holm EA, Hassold GN, Miodownik MA (2001) *Acta Mater* 49:2981
- Luo J (2007) *Crit Rev Solid State Mater Sci* 32:67
- Sano T, Saylor DM, Rohrer GS (2003) *J Am Ceram Soc* 86:1933
- Tanaka H, Kawai T (1996) *Surf Sci* 365:437
- Pojani A, Finocchi F, Noguera C (1999) *Surf Sci* 442:179
- Wilcox N, Ravilumar V, Rodrigues RP, Dravid VP, Vollmann M, Waser R, Soni KK, Adriaens AG (1995) *Solid State Ion* 75:127
- Fang PA, Gu H (2003) *Key Eng Mater* 247:323
- Yan MF, Cannon RM, Bowen HK (1983) *J Appl Phys* 54:764
- Chiang YM, Birnie DP III, Kingery WD (1996) *Physical ceramics: principles for ceramics science and engineering*. Wiley, New York
- Xing JJ, Wang XH, Gu H (2008) *J Chin Electr Microsc Soc* 27:5
- Shih SJ, Sergio LP, Cockayne DJH (2010) *J Mater Res* 25:260
- Cahn JW (1962) *Acta Metall* 10:789
- Bäurer M, Shih SJ, Bishop C, Harmer MP, Cockayne D, Hoffmann MJ (2010) *Acta Mater* 58:290
- Cho SG, Johnson PF (1994) *J Mater Sci* 29:4866. doi:[10.1007/BF00356536](https://doi.org/10.1007/BF00356536)
- Fossdal A, Einarsrud M-A, Grande T (2004) *J Solid State Chem* 177:2933
- Dillon SJ, Tang M, Craig Carter W, Harmer MP (2007) *Acta Mater* 55:6208
- Harmer MP (2010) *J Am Ceram Soc* 93:301
- Qian PX, Gu H, Aldinger F (2009) *Int J Mat Res* 99:240